A 3-axis PZT-based MEMS Gyroscope in 0.18µm CMOS

Imran Ahmed[1], David Halupka[1], Bertram Leesti[1], James A. Cherry[1], Rob McKenzie[1], Alireza Nilchi[2], Hamed Mazhab-Jafari[2], Martin Snelgrove[1], Raymond Chik[1]

[1]Kapik Integration, Toronto, Canada, E-mail: imran@kapik.com
[2]University of Toronto, Toronto, Canada

***Abstract*—A 3-axis interface for a PZT-based MEMS gyroscope uses a PLL-less architecture and does not require high-voltage devices nor charge-pumps. The use of PZT in the MEMS enables a low-cost package which does not require the MEMS to be vacuum sealed. A single amplifier is used to simultaneously amplify actuation and Coriolis signals, thereby maintaining orthogonal phase between the signals. The ASIC has an inherent Allan variance of 0.13 °/s/√Hz, and 1, 0.35, and 0.66 °/s/√Hz for the ASIC plus x, y, and z axes respectively. The ASIC utilizes 6.2mA of current and 6.22mm^2 of total area (including I/Os).**

I. Introduction

The recent growth of interactive user interfaces in mobile phones and video games has stimulated much demand for motion sensing devices such as gyroscopes. Existing MEMS-based gyroscopic sensors typically use electro-static based MEMS structures [1-4]. While these sensors can deliver good performance, they typically require expensive vacuum packaging to ensure high Q-factors, and/or require actuation voltages biased larger than the nominal supply voltage [1-4]. A PZT-based MEMS gyroscope [5] however, does not need expensive vacuum-sealing, and requires significantly smaller actuation voltages (~150mV p-p swing with 0.7V bias). This paper details the design of an interface ASIC for a 3-axis PZT-based MEMS gyroscope.

II. MEMS Gyroscope

The PZT MEMS structure used in this work consists of a suspended mass with a layer of PZT sandwiched between a top and bottom plate. As shown in Fig. 1, to sense x and y-axis rotation, a voltage at the MEMS's z-axis resonant frequency (29kHz) is applied to the four MEMS drive terminals (d_{x+}, d_{x-}, d_{y+}, and d_{y-}) which forces the mass to move along the z-axis. X-axis rotation contorts the PZT layer and super-imposes a differential current between the sense pins s_{y+} and s_{y-} that is proportional to the Coriolis force on the mass, amplitude-modulated at 29kHz and 90° out-of-phase with the actuation voltage. Y-axis rotation similarly results in differential current between s_{x+} and s_{x-} proportional to the y-axis Coriolis force.

Z-axis rotations are sensed as shown in Fig. 2. By applying a differential actuation voltage to a separate but identical MEMS on nodes d_{y+} and d_{y-} at the y-axis resonant frequency of 26kHz, the mass moves along the y-axis. Z-axis rotation contorts the PZT layers to induce a differential current between s_{x+} and s_{x-} amplitude-modulated at 26kHz and 90° phase-shifted relative to the actuation voltage.

The high mechanical-to-electrical sensitivity of PZT enables the MEMS to be manufactured with a very low Q-factor relative to electrostatic MEMS (~200 in this work compared to 36,000 [3]). The low Q-factor enables the PZT MEMS to be packaged at atmospheric pressure, resulting in reduced packaging costs – a key metric for devices such as gyroscopes which are used in large volumes for consumer applications. The high sensitivity of PZT allows for the mass to be actuated with a voltage biased at only 0.7V. By contrast, many electrostatic approaches require actuation voltages higher than the nominal supply voltage, necessitating charge pumps and/or the use of high voltage devices [1-4].

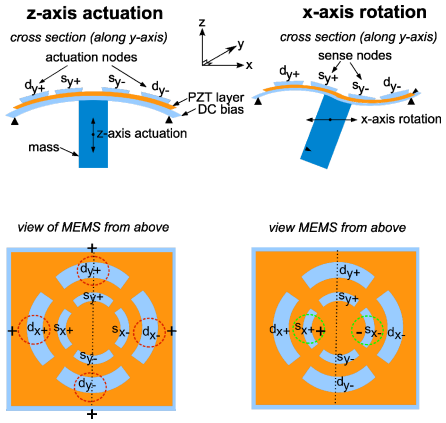

Fig. 1: MEMS actuation, and x/y-axis rotational sense illustration. Y-axis sensed similarly to x-axis but using pins s_{x+}, s_{x-}

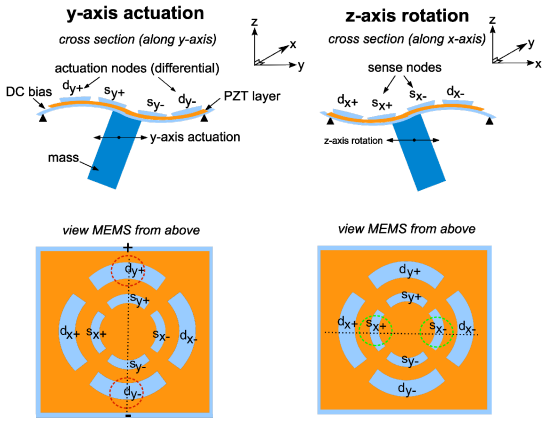

Fig. 2: MEMS actuation and z-axis rotation sense

III. MEMS ASIC INTERFACE

A. Overall architecture

Fig. 3 illustrates the overall architecture of the interface ASIC which performs the MEMS actuation and rotational sense/read-out.

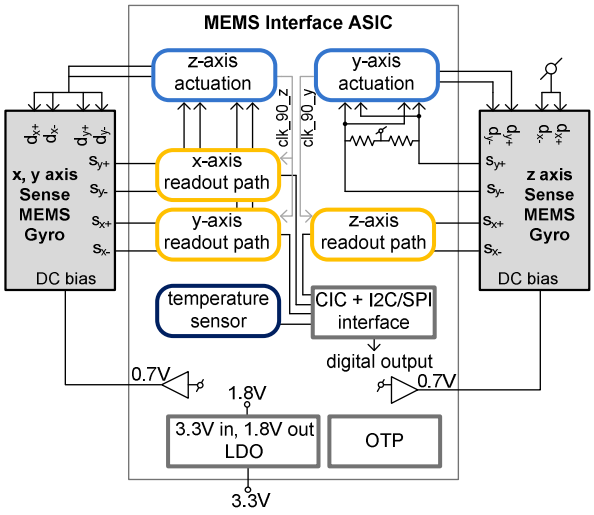

Fig. 3: MEMS gyroscope interface – overall architecture

All core circuits (actuation, read-out, and MEMS bias) operate from a 1.8V supply which is generated using an LDO from an off-chip 3.3V. To handle the 3.3V supply, the LDO uses thick-oxide devices. Configuration of the ASIC as well as read-out of the digital data is facilitated by the use of an I2C/SPI interface.

B. Actuation loop

Fig. 4 shows the detailed implementation of the MEMS actuation loop. The z-axis actuation and y-axis actuation loops each use identical copies of the circuit shown in Fig. 4. The inputs of the actuation loop are combined and rectified by an offset-compensated clipper and then filtered by a bi-quadriatic band-pass filter. A tuning algorithm is used to drive the 90° phase-shifted output (clk_90) of the filter to be orthogonal to the input of the filter. By applying a large voltage gain with zero phase-shift around the MEMS, Barkhausen's criteria for oscillation is satisfied, resulting in the actuation voltage oscillating at the resonant frequency of the MEMS. The MEMS itself is actuated with a signal derived from out_0, which has a 0° phase-shift from the band-pass filter's input at steady state.

An advantage of the actuation loop in this work is that: the clock required to mix the amplified Coriolis signal to baseband, which needs to be 90° out-of-phase to the actuation voltage, is readily available from the band-pass filter (clk_90). Hence, the approach used in this work has a reduced circuit complexity in comparison to prior MEMS gyroscope actuation loops, which use a separate PLL to generate the 90° phase shifted clock [1-4].

C. MEMS startup

An adaptive digital algorithm is used to trim the offset of the clipper-preamp in Fig. 4 such that the duty cycle of the clipped signal is 50%, thereby guaranteeing MEMS startup. A free-running ring-oscillator running at a frequency of 1 MHz is used to oversample the clipped MEMS actuation signal. In steady state, the number of high samples and low samples is equal (i.e. 50% duty cycle). However, in the presence of clipper input offset or the case of no oscillations, the high and low samples are not equal. Negative feedback is used to trim the input offset of the clipper to converge the duty cycle to 50%. If there are no oscillations at initial startup, negative feedback forces the clipper output to oscillate between high and low states, thereby injecting energy into the resonant MEMS to ensure MEMS startup.

D. MEMS voltage driver

The MEMS is actuated with a voltage driver (shown in Fig. 4) which has a low phase shift (~1°), and a programmable drive voltage of 150mV p-p nominally with a 0.7V DC bias. To enable the same buffer to be used for z-axis and y-axis actuation, the voltage buffer can be configured to convert a differential input into a single-ended voltage for z-axis actuation, or generate a differential drive voltage based on a differential input for y-axis actuation.

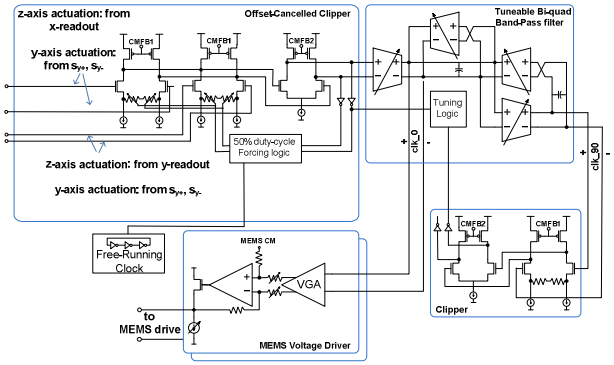

Fig. 4: Actuation loop in detail: Band-pass filter automatically tuned so that phase-shift through clipper, filter, and driver is 0°

E. Trans-impedance amplifier

Fig. 5 illustrates the Coriolis signal read-out path for x, y, and z-axes. An OTA with a differential g_m and a resistor divider in feedback applies trans-impedance amplification (TIA) of the Coriolis current signal. The TIA has a gain of ~800kΩ .The DC-bias of nodes s+ and s- is established using the feedback loop labeled $L_{in\text{-}cm}$. An advantage of this feedback loop is that: by tuning the value of R_{in1} relative to R_{in2}, off-axis mismatch in the MEMS can be compensated by presenting a counter-balanced impedance at the sense inputs. Thus off-axis induced coupling of the actuation signal into the differential sense nodes is minimized by adjusting R_{in1}.

For x and y axis rotation read-out paths, since d_{x+}, d_{x-}, d_{y+}, d_{y-} are simultaneously driven by the z-axis actuation voltage, a portion of the actuation voltage appears as common-mode

on the sense nodes s+ and s- as shown in Fig. 5. As a result, a buffered version of the z-axis actuation voltage appears at node v_{act}, and an amplified version at node v_{act_amp}. A significant advantage of the architecture used in this work is that: for x and y-axis read-out paths, a single amplifier can be used to simultaneously amplify the Coriolis signal and the z-axis actuation voltage. This reduces complexity and improves phase matching between actuation and read-out paths, in contrast to prior approaches that use independent carefully matched actuation and read-out paths for x and y axes [1-4].

As the z-axis actuation voltage is already amplified in the x and y read-out paths, the first stage of the clipper in Fig. 4 for z-axis actuation has a reduced impact in the phase separation between clk_90 and the amplified x and y–axis Coriolis signals, hence is designed to have 4× smaller power consumption compared to that used for y-axis actuation.

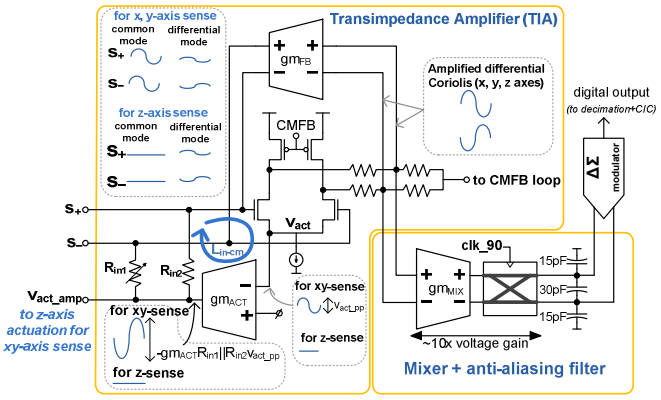

Fig. 5: Read-out path in detail

F. *Mixer + anti-aliasing filter*

As shown in Fig. 5, a chopper-based mixer using clk_90 as its carrier frequency is used to demodulate the amplified Coriolis signal to baseband. For x and y-axes rotational sense clk_90 comes from the z-axis actuation loop, and for z-axis rotational sense clk_90 comes from the y-axis actuation loop.

By distributing the gain of the read-out path such that the mixer+filter has DC gain of ~10x, the finite-gain-bandwidth property of a first order system is utilized to trade gain for reduced bandwidth, hence relaxing the size of the anti-aliasing filter capacitors (~1kHz 3dB-bandwidth using a total of 60pF of capacitance for each mixer).

G. *ADC*

The output of the mixer is digitized by a 3rd-order ΔΣ ADC. The ADCs for all axes' read-out paths are clocked at the z-axis actuation resonant frequency of 29kHz so as to ensure all motion sense data is synchronously sampled. To maximize linearity the ΔΣ modulator uses a 1-bit quantizer. The thermal noise floor of the ADC is designed such that the ADC achieves an SNR of 80dB with a 0.7V p-p differential input signal swing. Chopping is used in the opamps to minimize 1/f noise in the output. The ADC output is 16 bits wide (post CIC filtered), and output via an I2C/SPI interface.

H. *Temperature sensor*

The MEMS gyroscope itself has a temperature dependency which causes the MEMS gain and offset to vary with temperature. To compensate for temperature effects, fitting parameters which track the change in offset and gain of the MEMS+ASIC with temperature are measured at factory-test-time and stored in an on-chip OTP (One-Time-Programmable) memory. By using on-chip temperature measurements along with data stored in the OTP an end-user can compensate for temperature dependent effects in firmware.

The temperature sensor in this work uses a conventional PTAT voltage which is sampled by an ADC to produce a digital temperature reading as shown in Fig. 6. The temperature sensor is designed to be accurate to within ±1°C. To minimize the design effort, the same ADC used in the x, y, and z-axis read-out paths is also used in the temperature sensor.

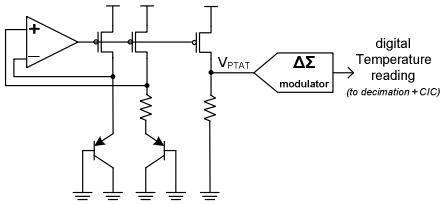

Fig. 6: Digital temperature sensor

IV. Measured Results

The 2.06mm × 3.02mm interface ASIC is implemented in a 3.3V/1.8V 0.18µm CMOS process. The chip consumes 6.2mA from a 3.3V off-chip supply. The two MEMS are intended to be stack wire-bonded onto the interface ASIC within one package, however measured results are based on a proof-of-concept prototype where the MEMS are packaged separately and PCB-connected to the ASIC. The ASIC has a full-scale of ±2000°/s, and output data rate of 100S/s.

Fig. 7 shows the Allan variance plots of the ASIC, x, y, and z-axis at 25°C. From Fig. 7, the Allan variance of the ASIC by itself (i.e. with the MEMS disconnected from the ASIC read-out path) is 0.13 °/s/√Hz. The Allan variance of the ASIC plus x, y, and z axes is 1, 0.35, and 0.66 °/s/√Hz respectively. It is noted that the noise levels of the x, y, and z axes read-outs are dominated by the MEMS itself.

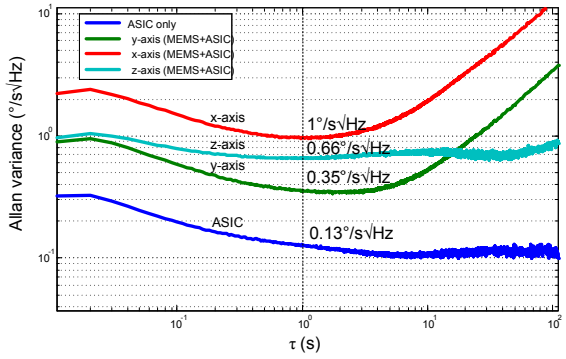

Fig. 7: Allan variance plot of x, y, z axis and ASIC by itself

Fig. 8 shows measured transient digital output of the x, y, and z channels when the system is subject to bursts of constant rotation on a rotary table at ±100°/s along the x, y, and z-axes. Note, the over/undershoots in the digital output are due an under-damped mechanical response in the rotary table itself, i.e. the ASIC+MEMS accurately captures transient high frequency rotational rates of the rate table.

Fig. 9 shows the measured temperature digital read-out vs. actual temperature for on-chip temperature sensor.

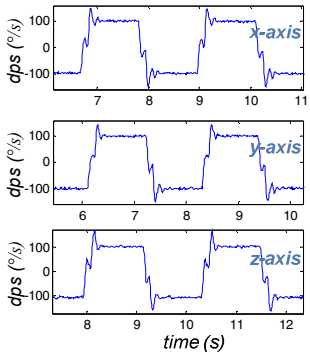

Fig. 8: Measured transient digital output of x, y, z-axis

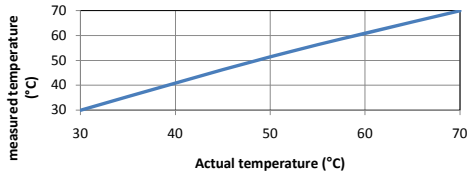

Fig. 9: On-chip digital temperature sensor measured results

Fig. 10 shows the measured un-compensated drift of the zero-rate-output (ZRO), and gain of the axes' digital output over temperature. Second-order polynomial curve fitting parameters based on the results of Fig. 9 and Fig. 10 are stored in OTP to be used by end-user firmware to compensate for gain and offset dependency on temperature. Fig. 11 shows micrographs of the ASIC and MEMS.

Table 1 compares the performance of this work with [1]-[4]. While prior works achieve higher sensitivity, this work achieves reasonable performance while realizing significantly smaller actuation voltages (thus not requiring a high-voltage process), hence minimizing production costs. This is favorable for the many consumer applications of gyroscopes which do not demand high sensitivity, but are sensitive to production costs.

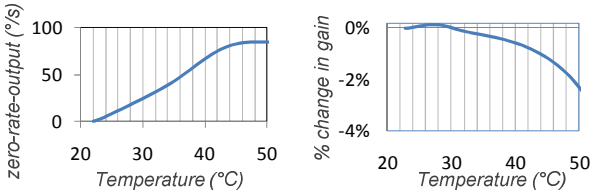

Fig. 10: Measured offset and gain variation with temperature

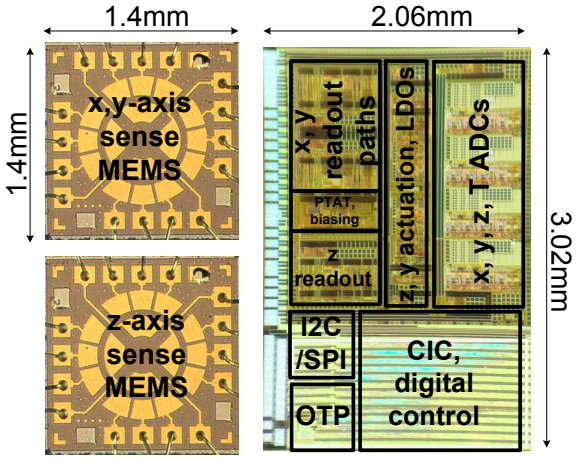

Fig. 11: Micrographs of Gyroscope MEMS and interface ASIC

Table 1: Comparison of works

Paper	# Axes	Current (mA)	Min. noise (°/s/√Hz)	MEMS Bias (V)	PLL?	Process	MEMS element
[1]	3	6.1	0.03	11	yes	0.13µm	Electrostatic
[2]	2	1.8	0.015	9.1	yes	0.35µm HVCMOS	Electrostatic
[3]	1	2	0.0001	40	yes	0.6µm	Electrostatic
[4]	1	64	0.001	10	yes	0.18µm HVCMOS	Electrostatic
This work	3	6.2	0.35	0.7	no	0.18µm	PZT

V. Conclusions

An ASIC interface for a PZT MEMS gyroscope was described. The PZT based MEMS enabled the interface to avoid using charge pumps as well as costly vacuum packaging. A PLL-less architecture for the MEMS actuation loop was described, as well as a single amplifier in the read-out path which enabled well matched simultaneous amplification of read-out and MEMS actuation signals. Measured results from a prototype in 1.8/3.3V 0.18µm CMOS showed the ASIC to achieve an inherent Allan variance of 0.13 °/s/√Hz.

References

[1] L. Prandi et al, "A Low-Power 3-Axis Digital-Output MEMS Gyroscope with Single Drive and Multiplexed Angular Rate Readout", in *IEEE Int. Solid-State Circuits Conf. Dig. Tech. Papers*, 2011, pp. 104-105

[2] L. Aaltonen et al, "Pseudo-Continuous-Time Readout Circuit for a 300°/s Capacitive 2-Axis Micro-Gyroscope", *IEEE J. Solid-State Circuits*, vol. 44, no. 12, pp. 3609-3620, December 2009.

[3] A. Sharma, M.F. Zaman, F. Ayazi, "A Sub -0.2°/hr Bias Drift Micromechanical Silicon Gyroscope With Automatic CMOS Mode-Matching," *IEEE J. Solid-State Circuits*, vol. 44, no. 5, pp. 1593-1608, May 2009.

[4] A. Elsayed et al, "A Self-Clocked ASIC Interface for MEMS Gyroscope with 1m°/s/√Hz Noise Floor", *IEEE Custom Integrated Circuits Conference*, 2011, pp. 1

[5] K. Okada, et al, "Development of 6-axis Motion Sensors Using Piezoelectric Elements," *Proceedings of the 21st Sensor Symposium*, pp. 385-390, 2004.